Journal of Solid State Chemistry 181 (2008) 3078–3085

Contents lists available at ScienceDirect

Journal of Solid State Chemistry

journal homepage: www.elsevier.com/locate/jssc

Structure and luminescence properties of silver-doped $NaY(PO_3)_4$ crystal

M. El Masloumi [a,b], V. Jubera [a], S. Pechev [a], J.P. Chaminade [a], J.J. Videau [a,*], M. Mesnaoui [b], M. Maazaz [b], B. Moine [c]

[a] CNRS, Université Bordeaux, ICMB, 87 Avenue du Dr A. Schweitzer, Pessac F-33608, France
[b] Faculté des Sciences Semlalia, LC S M, Marrakech, Maroc
[c] Université Claude -Bernard, Lyon 1, L PCM L, 10 rue A.M. Ampère, Villeurbanne F-69622, France

ARTICLE INFO

Article history:
Received 21 May 2008
Received in revised form
24 July 2008
Accepted 25 July 2008
Available online 19 August 2008

Keywords:
Phosphate
Crystal
Luminescence
Silver

ABSTRACT

Single crystals of $NaY(PO_3)_4$ and $Ag_{0.07}Na_{0.93}Y(PO_3)_4$ have been synthesized by flux method. These new compounds turned out to be isostructural to $NaLn(PO_3)_4$, with Ln = La, Nd, Gd and Er [monoclinic, $P2_1/n$, $a = 7.1615(2)$ Å, $b = 13.0077(1)$ Å, $c = 9.7032$ (3) Å, $\beta = 90.55$ (1)°, $V = 903.86(14)$ Å^3 and $Z = 4$]. The structure is based upon long polyphosphate chains running along the shortest unit-cell direction and made up of PO_4 tetrahedra sharing two corners, linked to yttrium and sodium polyhedra. Infrared and Raman spectra at room temperature confirms this atomic arrangement. The luminescence of silver ions was reported in metaphosphate of composition $Ag_{0.07}Na_{0.93}Y(PO_3)_4$. One luminescent centre was detected and assigned to single Ag^+ ions.

1. Introduction

Many works about the relationships between the structure and the luminescent properties of the silver ion have been carried out in the condensed phosphates $AgM(PO_3)_3$ (M = Mg, Zn, Ba) [1] and in the diphosphates $Na_{2-x}Ag_xZnP_2O_7$ [2], where two luminescent centres (single Ag^+ and Ag^+–Ag^+ pairs) have been correlated with the symmetry of the silver sites. In the same way, condensed phosphates with the general formula $M^IM^{III}(PO_3)_4$ (M^I = monovalent cation, M^{III} = rare earth) were published mainly for their optical properties. For instance, $KNd(PO_3)_4$ crystal is not only potentially useful as laser material for miniature laser devices [3], but also has attractive performances to non-linear optical process [4]. In order to enrich this family of compounds, we successfully synthesized the solid state compound $NaY(PO_3)_4$. The phase diagram of $Y(PO_3)_3$–$NaPO_3$ is known [5,6]. In the first reference, an intermediate compound of formula $NaY(PO_3)_4$ and obtained by recrystallization is reported. However, the X-ray characterization results presented by the authors are completely different from those we obtained. In the second reference, it has been discovered that the initial phosphates, $Y(PO_3)_3$ and $NaPO_3$, react, respectively, at the 1:2 molar ratio forming a double metaphosphate with the formula $Na_2Y(PO_3)_5$ for which the X-ray diffraction pattern is similar to the phase that we have obtained. In both cases no detailed structural study was undertaken to confirm the exactitude of these phases.

In this context, our research initially consists in the synthesis and the structural determination of the $NaY(PO_3)_4$ crystal in order to try to remove this confusion ambiguity. At the same time, Ag-doped $NaY(PO_3)_4$ crystal is synthesized and this structure has been compared to the one of Ag-free $NaY(PO_3)_4$ crystal. Additional characterizations by micro-Raman and infrared (IR) spectroscopy are reported for the two phosphate crystals. Ag-doped $NaY(PO_3)_4$ single crystal is studied by photoluminescence spectroscopy and the use of the emission decay allows to identify the silver emitter centres.

2. Experimental

2.1. Crystal growth

Single crystals of $NaY(PO_3)_4$ and of silver-doped $Ag_xNa_{1-x}Y(PO_3)_4$ were prepared by flux method using the reagents Y_2O_3 (99.99%), $NH_4H_2PO_4$ (98%) and Na_2CO_3 (99+%) and $AgNO_3$ (99.9+%) (molar ratio Na/Ag close to 10 for silver-doped crystal). At high temperature, the single crystals were obtained by spontaneous crystallization during slow cooling of a mixture containing excess of Na_2O (Ag_2O) and P_2O_5 with regard to the composition $NaY(PO_3)_4$ or ($Ag_xNa_{1-x}Y(PO_3)_4$) in the ternary phase diagram $38Na_2O(xAg_2O)$–$56P_2O_5$–$6Y_2O_3$. The thermal cycle is the following:

* Corresponding author.
E-mail address: videau@icmcb-bordeaux.cnrs.fr (J.J. Videau).

0022-4596/$ - see front matter © 2008 Elsevier Inc. All rights reserved.
doi:10.1016/j.jssc.2008.07.040

the mixture transferred to a platinum crucible was preheated at low temperature of 200 °C for 6 h,
then, the temperature was progressively increased up to 750 °C and was maintained for 12 h,
the obtained crystals were isolated after a cooling down to 450 °C (2 °C h^{-1}) and then to room temperature (50 °C h^{-1}).

Single crystals were separated by washing with dilute nitric acid (1 mol l^{-1}). It should be specified that we successively obtained YP_3O_9 crystals at about 1000 °C and YPO_4 crystals beyond 1230 °C with the same flow composition. The morphology of $NaY(PO_3)_4$ crystals is shown in Fig. 1, for example.

2.2. Structure refinement

The single-crystal X-ray measurements of $NaY(PO_3)_4$ and $Ag_xNa_{1-x}Y(PO_3)_4$ were performed on a Bruker Kappa CCD diffractometer with a graphite monochromator using Mo$K\alpha$ radiation. The chemical crystal data, the parameters used for the X-ray diffraction data collection and the results of crystal structure determinations of $NaY(PO_3)_4$ and $Ag_{0.07}Na_{0.93}Y(PO_3)_4$ are listed in Table 1. The empirical absorption corrections were carried out using SCALEPACK programme [7]. Both structures were solved by direct methods and refined by full-matrix least-squares on F^2 values using SHELXL97 [8]. The final atomic coordinates with the equivalent isotropic displacement parameters of $NaY(PO_3)_4$ are reported in Table 2. Selected interatomic distances are listed in Table 3. The refined atomic positions of a silver containing single-crystal $Ag_xNa_{1-x}Y(PO_3)_4$ are those of $NaY(PO_3)_4$ where Ag partly substitutes for Na in agreement with the presence of a residual electronic density existing in the sodium site of Ag-free crystal. The substitution ratio was established to be $x = 0.07(1)$ with a corresponding formula $Ag_{0.07}Na_{0.93}Y(PO_3)_4$.

2.3. Vibrational spectroscopy

The IR spectra of a mixture of KBr powder and powdered samples of $NaY(PO_3)_4$ and $Ag_{0.07}Na_{0.93}Y(PO_3)_4$ (3% weight) were recorded by the diffuse reflection technique using a Bruker IFS Equinox 55FTIR spectrometer (signal averaging 30 scans at a resolution of 4 cm^{-1}) in the range of 1500–400 cm^{-1}.

The Raman spectrum of crystal sample was recorded with a Labram confocal micro-Raman instrument from Jobin–Yvon

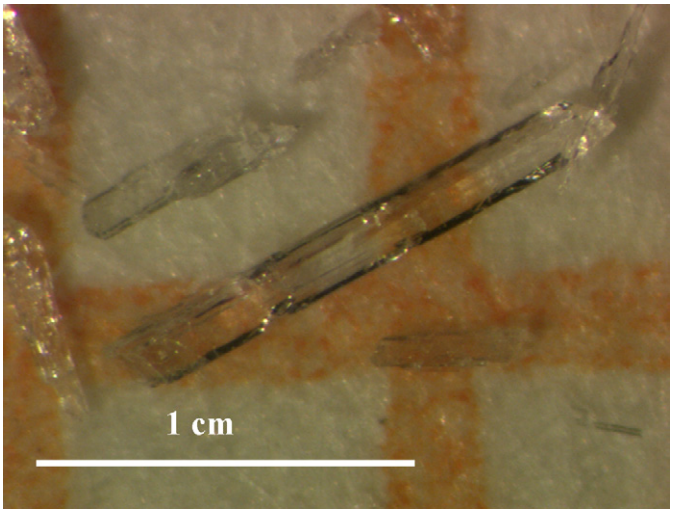

Fig. 1. Single crystals $NaY(PO_3)_4$ prepared by flux method.

Table 1
Crystal data and structure refinement for $NaY(PO_3)_4$ and $Na_{0.93}Ag_{0.07}Y(PO_3)_4$

Crystal data		
Empirical formula	$NaY(PO_3)_4$	$Na_{0.93(1)}Ag_{0.07(1)}Y(PO_3)_4$
Space group	$P2_1/n$	$P2_1/n$
Z	4	4
Temperature (K)	293(2)	293(2)
Formula weight (g mol^{-1})	427.78	433.72
Unite cell dimensions		
a (Å)	7.1615(2)	7.1638 (1)
b (Å)	13.0077(1)	13.0105(2)
c (Å)	9.7032 (3)	9.6990(1)
β (deg)	90.55 (1)	90.59(1)
Volume (Å^3)	903.86 (2)	903.94(2)
D_X (g cm^{-3})	3.144	3.206
$F(000)$	824	838
Crystal size	$0.01 \times 0.02 \times 0.1$ mm^3	$0.05 \times 0.052 \times 0.3$ mm^3
Data collection		
Radiation	Mo$K\alpha$ ($\lambda = 0.71073$ Å)	Mo$K\alpha$ ($\lambda = 0.71073$ Å)
Monochromator	Graphite	Graphite
Diffractometer	Bruker Kappa CCD	Bruker Kappa CCD
Absorption coefficient (mm^{-1})	7.28	7.48
θ range (deg)	3.47–32.01	3.25–32.02
Index ranges	$-10<h<10$ $-18<k<18$ $-13<l<13$	$-10<h<10$ $-19<k<19$ $-14<k<14$
Scan type	Φ/Ω	Φ/Ω
Reflections collected [$I>2\sigma(I)$]	6394	10,459
Independent reflections [$I>2\sigma(I)$]	1929	2873, $R_{int} = 0.0291$
Refinement		
Refinement method	Full-matrix L.S. on F^2	Full-matrix L.S. on F^2
Data/restraints/unique	1929/0/164	2873/0/165
Weighting scheme	$\omega = 1/[\sigma^2(F_o^2)+(\alpha P)+\beta P]$, where $P = (F_o^2+2F_c^2)/3$	$\omega = 1/[\sigma^2(F_o^2)+(\alpha P)+\beta P]$, where $P = (F_o^2+2F_c^2)/3$
α	0.0698	0.027
β	0.57	0.81
Absorption correction	Multi-scan	Multi-scan
Extinction coefficient	0.0114 (17)	0.0046 (5)
Goodness-of-fit	1.319	1.101
Final R indices [$I>2\sigma(I)$]		
R_1	0.0481	0.0235
wR_2	0.1297	0.0549
Largest diff. peak and hole (e Å^{-3})	1.34 (O_4), −1.36 (O_5)	0.569 and 0.717

(typical resolution of 4 cm^{-1}), in backscattering geometry at room temperature. The system consists of a holographic notch filter for Rayleigh rejection, a microscope equipped with 10×, 50× and 100× objectives (the latter allowing a spatial resolution of less than 2 mm), and CCD detector. The source used for excitation was an Argon laser, with an output power of about 10 mW at 514.5 nm.

2.4. Photoluminescence

UV luminescent properties were studied at room temperature, using a SPEX Fluorolog FL 212 spectrofluorimeter. Excitation spectra were corrected from the variation of the incident flux as well as emission spectra from the transmission of the monochromator and from the response of the photomultiplier. The decay curves have been recorded at room temperature with a

Table 2
Atomic coordinates, occupancy rate, equivalent displacement parameters (Å^2) of $NaY(PO_3)_4$

	Site	Site symmetry	x	y	z	U_{eq}
Y	4*e*	1	0.51249 (8)	0.21886 (5)	0.97645 (5)	0.0077 (2)
Na	4*e*	1	0.99953 (39)	0.22206 (25)	0.06331 (33)	0.0211 (7)
P1	4*e*	1	0.26696 (21)	0.09131 (13)	0.70092 (18)	0.0078 (4)
P2	4*e*	1	0.64842 (22)	0.12825 (12)	0.30374 (17)	0.0073 (3)
P3	4*e*	1	0.24955 (21)	0.10228 (12)	0.24495 (18)	0.0076 (4)
P4	4*e*	1	0.87473 (22)	0.11503 (12)	0.76312 (18)	0.0075 (4)
O1	4*e*	1	0.23652 (62)	0.16238 (38)	0.58346 (51)	0.0125 (10)
O2	4*e*	1	0.42823 (61)	0.11164 (36)	0.79477 (51)	0.0125 (10)
O3	4*e*	1	0.08515 (61)	0.08021 (36)	0.79395 (49)	0.0111 (9)
O4	4*e*	1	0.71979 (66)	0.02100 (34)	0.36452 (49)	0.0106 (9)
O5	4*e*	1	0.72537 (61)	0.21109 (35)	0.39303 (49)	0.0112 (10)
O6	4*e*	1	0.67762 (63)	0.13214 (38)	0.15278 (50)	0.0128 (10)
O7	4*e*	1	0.43032 (60)	0.12637 (35)	0.33671 (48)	0.0097 (9)
O8	4*e*	1	0.28564 (62)	0.10925 (37)	0.09424 (49)	0.0114 (10)
O9	4*e*	1	0.09267 (61)	0.16655 (35)	0.29726 (49)	0.0107 (9)
O10	4*e*	1	0.78269 (66)	0.01297 (34)	0.70807 (51)	0.0116 (10)
O11	4*e*	1	0.86753 (63)	0.18881 (37)	0.64779 (51)	0.0124 (10)
O12	4*e*	1	0.79514 (62)	0.14770 (36)	0.89728 (49)	0.0110 (10)

Table 3
Selected lengths (Å) in $NaY(PO_3)_4$

Y–O		Na–O	
Y–O11_k	2.306(5)	Na1–O12_a	2.372(6)
Y–O2	2.323(5)	Na1–O1_d	2.419(5)
Y–O6_f	2.358(5)	Na1–O9_f	2.468(6)
Y–O12	2.361(4)	Na1–O5_d	2.481(6)
Y–O9_k	2.365(5)	Na1–O8_f	2.536(6)
Y–O5_j	2.384(4)	Na1–O6	2.734(6)
Y–O1_k	2.451(5)	Na1–O11_d	2.987(5)
Y–O8_I	2.452(1)	Na1–O7_d	2.991(6)
P–O		P–O	
P1–O1	1.482(5)	*P3–O8*	1.490(5)
P1–O2	1.488(5)	P3–O9	1.493(5)
P1–O4_e	1.596(5)	P3–O10_e	1.584(5)
P1–O3	1.598(5)	P3–O7	1.595(5)
P2–O6	1.483(5)	P4–O11	1.475(5)
P2–O5	1.485(5)	P4–O12	1.488(5)
P2–O4	1.597(5)	P4–O10	1.573(5)
P2–O7	1.597(5)	P4–O3_f	1.599(5)
Na–Na		Y–Y	
Na–Na	5.907(3)	Y–Y	5.715(3)

Operators for generating equivalent atoms: $a = x, y, z-1$; $b = x+1, y, z-1$; $c = x-1/2, -y+1/2, z-1/2$; $d = x+1/2, -y+1/2, z-1/2$; $e = -x+1, -y, -z+1$; $f = x+1, y, z$; $g = x-1, y, z$; $h = x-1, y, z+1$; $i = x, y, z+1$; $j = x-1/2, -y+1/2, z+1/2$; $k = x+1/2, -y+1/2, z+1/2$.

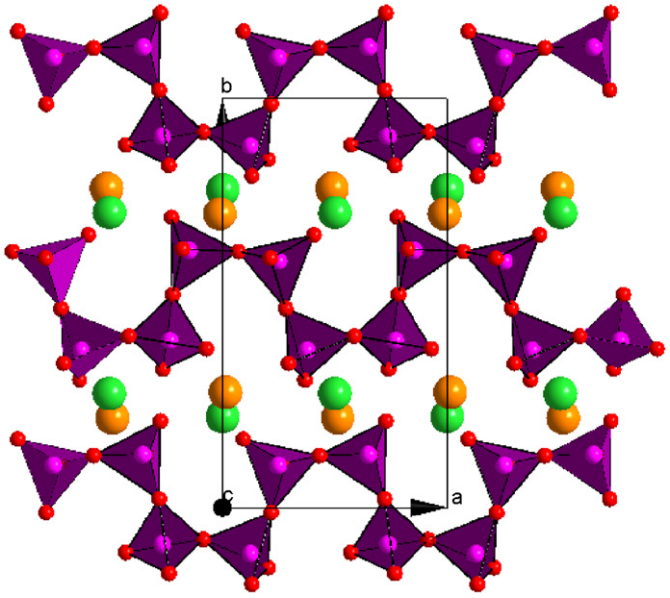

Fig. 2. Projection in *ab* plane of the Ag-free or -doped $NaY(PO_3)_4$ structure; Na or Ag and Y atoms are presented by green and yellow spheres, respectively.

multicanal analyser SR 430 Stanford Research via Trial 190 Jobin–Yvon monochromater with PM 97 89 EMI as detector under excitation obtained by a YAG laser with OPO system.

3. Results and discussion

3.1. Structure description of $NaY(PO_3)_4$ and $Ag_{0.07}Na_{0.93}Y(PO_3)_4$

Projection on *ab* plane is depicted in Fig. 2. The basic structure units of $NaY(PO_3)_4$ and $Ag_{0.07}Na_{0.93}Y(PO_3)_4$ are two meandering chains formed by corner-sharing PO_4 tetrahedra with the $(PO_3)^-$ formula. The $(PO_3)_n^-$ chains (two per unit cell) run along the *a* direction. In PO_4 tetrahedra, the P–O distances vary between 1.475(5) and 1.599(5) Å, and the shortest distances correspond to the non-bridging P–O connections, whereas the largest ones are along the P–O bridges. These chains are interconnected by Y and Na or Ag polyhedra forming a three-dimensional framework. The yttrium atom is surrounded by eight oxygen atoms with the Y–O bond distances ranging between 2.306(5) and 2.452(1) Å which compare well with the values reported for $NaLn(PO_3)_4$ (Ln = La, Nd, Gd, Er) [9–12]. As a result of our investigations, Ag- free or -doped $NaY(PO_3)_4$ appear to be isostructural with $NaLa(PO_3)_4$, $NaNd(PO_3)_4$, $NaGd(PO_3)_4$ and $NaEr(PO_3)_4$.

The YO_8 polyhedra, which are slightly distorted antiprisms, are isolated from each other. The shortest Y–Y distance is 5.715(3). Fig. 3 shows that when the radius of the Ln^{3+} cation decreases from La to Er, the cell volume decreases. However, the *Ln–Ln* distance remains almost constant [d_{La-La}(5.734 Å) [9] ≈ d_{Nd-Nd}(5.719 Å) [10] ≈ d_{Gd-Gd}(5.705) [11] ≈ d_{Y-Y}(5.715 Å) ≈ d_{Er-Er}(5.712 Å) [12]].

The evolution of the sodium or silver environment is much more interesting and it is worth lingering over it. The first coordination sphere of the Na or Ag atom is composed of six oxygen atoms, all of them being non-bridging with respect to the

$(PO_3)^-_n$ chains. The Na (Ag)–O bond lengths within this first coordination sphere do not vary very much over the series of Ln^{3+}-based compounds under consideration [9–12]. However, if we consider the bond valences in $NaLa(PO_3)_4$ (Table 4), there is a seventh oxygen atom-O11, with a weaker but worthy-of-interest contribution to the Na coordination. So the latter was assumed to be seven [9], so was in $NaNd(PO_3)_4$ [10]. Comparatively, in Ag-free and -doped $(NaYPO_3)_4$, sodium is coordinated to eight close-enough oxygen atoms forming an irregular $Na(Ag)O_8$ polyhedron (Fig. 4). It is interesting to note that the eighth oxygen-O7, is the first bridging oxygen atom of $(PO_3)^-_n$ chain to join the Na (Ag)-polyhedron. A careful observation of the Na (Ag)–O7 interatomic distance over five isostructural $NaLn(PO_3)_4$ compounds (Table 5) shows clearly that it reduces as the rare-earth atom is getting smaller. Starting from $NaGd(PO_3)_4$ the corresponding bond valence (0.035) becomes significant enough so as to consider Na (Ag) as eight coordinated.

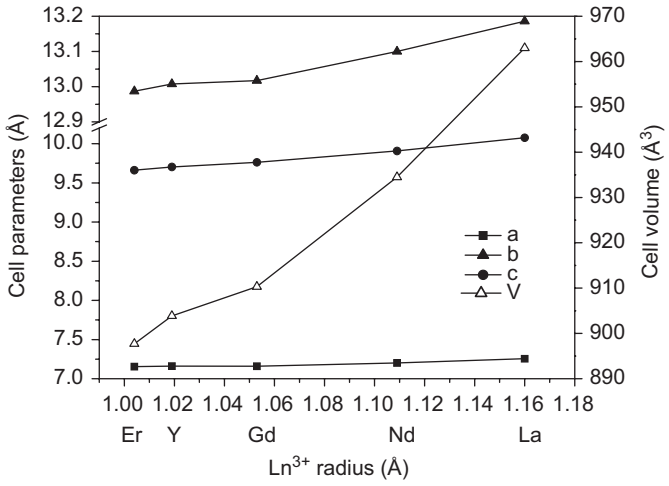

Fig. 3. Evolution of cell parameters [a (■), b (▲) and c (●)] and volume [V (△)] in $NaLn(PO_3)_4$ (Ln: La, Nd, Gd, Y and Er) as a function of Ln radius.

Table 4
Length (Å) and bond valence of Na–O_B (bridging oxygen) and Na–O_{NB} (non-bridging oxygen) bonds in the $NaY(PO_3)_4$ and $NaLa(PO_3)_4$ crystal structures

Oxygen atoms	$NaY(PO_3)_4$		$NaLa(PO_3)_4$ [9]	
	Na–O (Å)	Bond valence	Na–O (Å)	Bond valence
$O12_{NB}$	2.372	0.215	2.398	0.200
$O1_{NB}$	2.419	0.189	2.464	0.168
$O9_{NB}$	2.468	0.166	2.482	0.160
$O5_{NB}$	2.481	0.160	2.479	0.161
$O8_{NB}$	2.536	0.138	2.583	0.121
$O6_{NB}$	2.734	0.081	2.749	0.078
$O11_{NB}$	2.987	0.041	3.050	0.034
$O7_B$	2.991	0.04	(3.215)	(0.022)

3.2. *Vibrational characterization of $NaY(PO_3)_4$ and $Ag_{0.07}Na_{0.93}Y(PO_3)_4$*

$NaY(PO_3)_4$ and $Ag_{0.07}Na_{0.93}Y(PO_3)_4$ possess a primitive unit with a monoclinic structure (space group $P2_1/n$) with four molecular units. The meandering metaphosphate chains consist of corner-sharing PO_4 groups and all atoms are located in general position on C_1 sites. The Ag-free or -doped $NaY(PO_3)_4$ cell contains therefore $18 \times 4 = 72$ atoms that give $72 \times 3 = 216$ vibrational modes in which three acoustic modes are included. Correlation of the symmetry species for C_1 sites to the C_2^5h factor group leads to the irreducible representations of all the modes in $Na(Ag)Y(PO_3)_4$ as follows:

$$\Gamma_{\text{vib. Na(Ag)Y(PO}_3)_4} = 54\text{Ag} + 54\text{Au} + 54\text{Bg} + 54\text{Bu}.$$

The external modes include the optical translations (lattice vibrations) of four PO_4 ion groups and of two cations [Na^+ or Ag^+ and Y^{3+}] and the rotations (librations) of PO_4 tetrahedra. No rotational modes are possible with a monoatomic ion.

Table 5
Length (Å) and bond valence of Na–O(7) bonds in the isostructural family $NaLn(PO_3)_4$ (Ln = La, Nd, Gd, Y and Er)

Ln	Na–O(7)	Bond valence	Refs.
La	3.215	0.022	[9]
Nd	3.123	0.028	[10]
Gd	3.046	0.035	[11]
Y	2.991	0.040	This work
Er	2.975	0.042	[12]

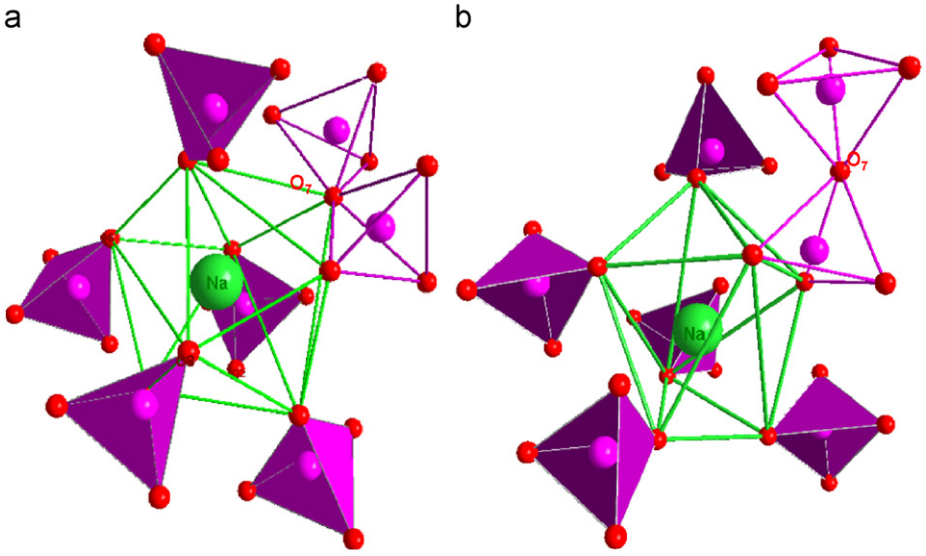

Fig. 4. Coordination polyhedron of Na or Ag atom in Ag-free or -doped $NaY(PO_3)_4$ (a) and $NaLa(PO_3)_4$ (b).

The irreducible representations of optical translations, rotations and acoustic modes are, respectively:

- $\Gamma_{trans.} = 18Ag+18Bg+17Au+16Bu$,
- $\Gamma_{rot.} = 12Ag+12Bg+12Au+12Bu$,
- $\Gamma_{ac.} = 1Au+2Bu$.

After subtraction, the irreducible representations corresponding to the internal modes of the metaphosphate chains are the following: $\Gamma_{int.} = 24Ag\,(Ra)+24Bg\,(Ra)+24Au\,(IR)+24Bu\,(IR)$ which includes

the PO_2 stretching modes: $\Gamma_{PO_2 stret.} = 8Ag\,(Ra)+8Bg\,(Ra)+8Au\,(IR)+8Bu\,(IR)$, including 16 antisymmetric $\nu asPO_2$ (8 Ra and 8 IR) modes and 16 symmetric νsPO_2 (8 Ra and 8 IR) modes,
the POP stretching modes: $\Gamma_{POP\ stret.} = 4Ag\,(Ra)+4Bg\,(Ra)+4Au\,(IR)+4Bu\,(IR)$ including 8 antisymmetric $\nu asPOP$ (4 Ra and 4 IR) modes and 8 symmetric $\nu sPOP$ (4 Ra and 4 IR) modes,
the remaining internal modes, i.e. 12Ag(Ra)+12Bg(Ra)+12Au(IR)+12Bu(IR), correspond to the bending modes $\delta(PO_2)$ and $\delta(POP)$.

Table 6
Band assignment (cm^{-1}) for $NaY(PO_3)_4$ crystal, for example

IR	Raman	Assignment
1382w		$\nu sPO_2+\nu asPO_2$
1319w		
1296s		
1263sm	1266vw	
1232sm	1235m	
1205m	1229w	
	1207w	
1192m	1190vs	
1162w	1175vw	
1140s	1131vw	
	1120w	
1116s	1117vw	
1093w	1097vw	
1074s	1073vw	
1068s	1066vw	
1062vs	1051vw	
1045w	1040vw	
	1020vw	
1014m	1013m	
		$\nu asPOP+\nu sPOP$
1003w	1005vw	
968vw		
916vs		
860w		
827w	817vw	
	811vw	
800s	799w	
792m		
761vs	768w	
729s	720m	
	703s	
688m		
646vw		$\delta PO_2+\delta POP$+external modes
630w		
611m	606vw	
586s	581w	
578w		
567m	566vw	
	553vw	
530vs	534vw	
511vs	522w	
	506w	
474s	466vw	
455w	457vw	
449m	444vw	
	433m	
410m	406vw	
	390w	
	376w	
	361w	
	355w	
	319vw	
	323w	
	297m	
	241vw	
	218w	
	205vw	
	190vw	
	184w	

Note: vs:very strong, s:strong, m:medium, w:weak, vw:very weak.

$NaY(PO_3)_4$ and $Ag_{0.07}Na_{0.93}Y(PO_3)_4$ show the same IR and Raman spectra. For example, those of Ag-free $NaY(PO_3)_4$ are, respectively, presented in Figs. 5 and 6. The frequencies of $(O_{1/2}PO_2O_{1/2})^-$ anion with $(PO_3)^-$ formula in chain metaphosphates are assigned to the $(PO_2)^-$ species and P–O–P bridge. Both band (IR) and line (Ra) number are almost identical to that of the theoretical prediction as shown in Table 6. The bands and lines observed in the regions 1000–1300 and 650–1000 cm^{-1} can be, respectively, attributed to the antisymmetric and the symmetric stretching vibrations (νas and νs) of $(PO_2)^-$ species and to POP bridges [13,14]. It is generally admitted that the symmetry stretching vibrations (νsPOP) in chain metaphosphate occur in the range close to 700 cm^{-1} as strong Raman lines and weak IR bands. The antisymmetric modes (νasPOP) are located around 900–800 cm^{-1} and give rise to strong IR bands and weak Raman lines. In the low-frequency region below 650 cm^{-1}, it is very difficult to distinguish the antisymmetric (δas) and symmetric (δs) bending modes $(PO_2)^-$ species and (δPOP) bending. Moreover, these modes overlay with external modes. All of these bands are characteristic of infinite chain of PO_4 tetrahedra bound by bridging oxygen. A comparison of the Raman and IR positions of bands (see Table 6) shows that the majority of them are not coincident; this fact is in agreement with the centrosymmetric structure of Ag-free and -doped $NaY(PO_3)_4$.

4. Photoluminescence investigation of $Ag_{0.07}Na_{0.93}Y(PO_3)_4$

As mentioned in the introduction, the aim of the present work is the study of the structure and luminescent centres in silver-doped $Ag_{0.07}Na_{0.93}Y(PO_3)_4$ crystal. This composition was selected as model system between low and high activator concentration.

4.1. Experimental results

No luminescence was detected in the Ag-free $NaY(PO_3)_4$. Fig. 7 shows the normalized excitation ($\lambda_{em} = 360$ nm) and emission ($\lambda_{exc} = 225$ nm) spectra of $Ag_{0.07}Na_{0.93}Y(PO_3)_4$ crystal recorded at room temperature and peaking at 225 and 360 nm respectively. It is noteworthy the shape dissymmetry of the emission band (Fig. 7, inset) and consequently it must be investigated in a more detailed way. Fig. 8 presents the emission spectra under excitations at 222, 225 and 230 nm. A comparison between them shows great difference, two main components can be distinguished. This inhomogeneous width is comparable with emission bands in glass and the maximum is slightly red shifted as the selected excitation wavelength increases. Indeed, the excitation at 222 nm favours the radiative de-excitation peaking at about 345 nm, the one at 230 nm leads to the emission with maximum at about 360 nm. Under excitation at 225 nm gives rise to an emission band peaking at 353 nm with the maximum of intensity and the greater width.

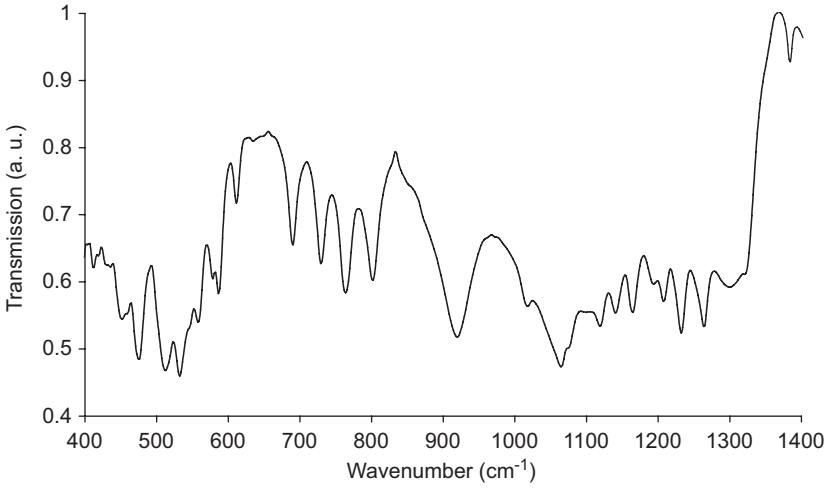

Fig. 5. FT-IR spectrum of $NaY(PO_3)_4$.

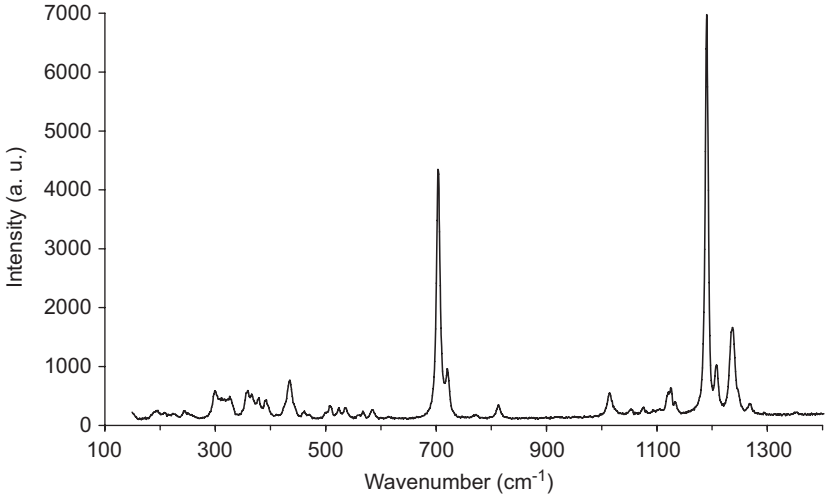

Fig. 6. Raman spectrum of $NaY(PO_3)_4$.

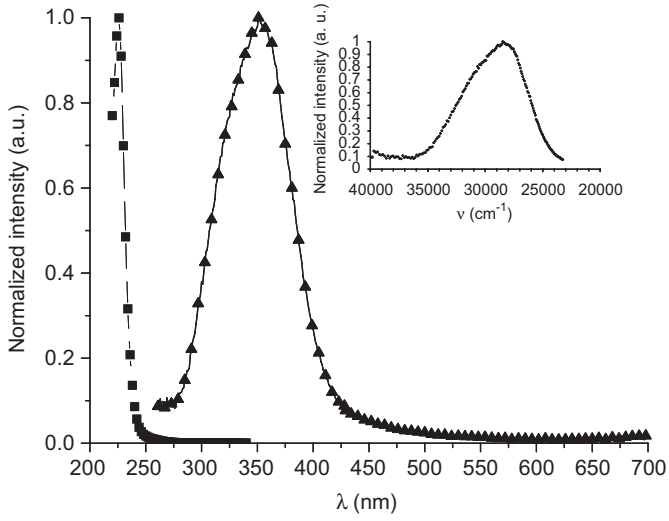

Fig. 7. Excitation [$\lambda_{em} = 360$ nm (■)] and emission [$\lambda_{exc} = 225$ nm (▲)] of Ag^+ ions in $Ag_{0.07}Na_{0.93}Y(PO_3)_4$ crystal recorder at room temperature. The inset shows the emission ($\lambda_{exc} = 225$ nm) vs energy (cm^{-1}).

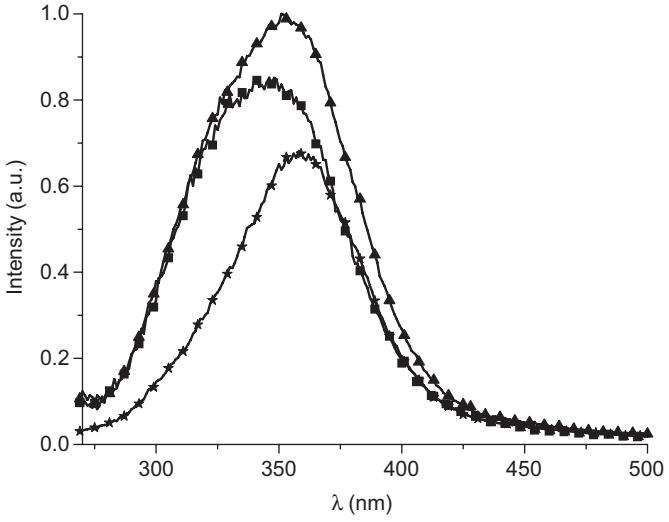

Fig. 8. Emission spectra of the Ag^+ ions in $Ag_{0.07}Na_{0.93}Y(PO_3)_4$ crystal under 222 nm (■), 225 nm (▲) and 230 nm (★) excitations recorded at room temperature.

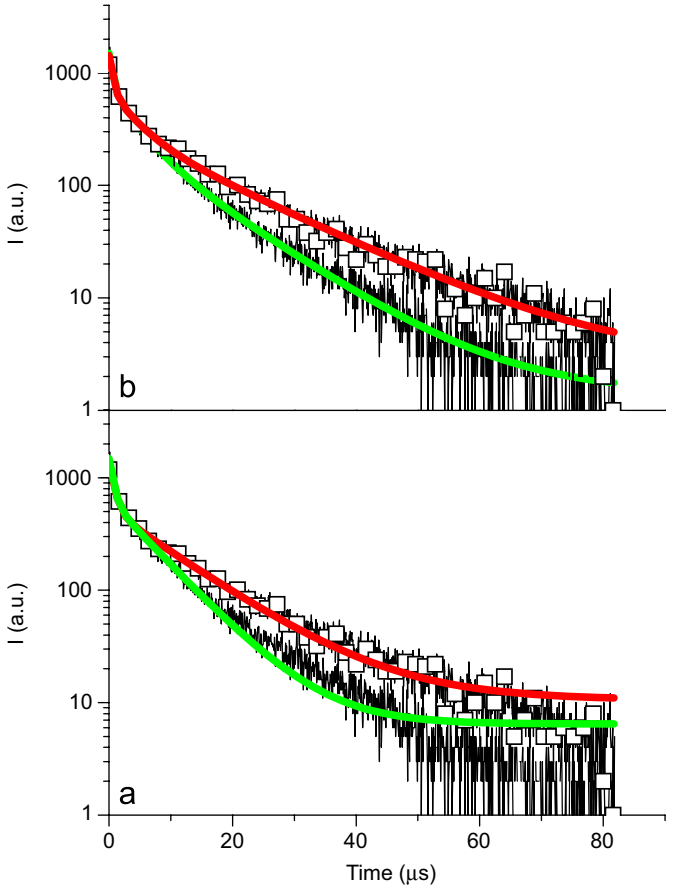

Fig. 9. Emission decay, recorded at room temperature, with laser excitation at 222 and 230 nm detected at 310 nm (—) and 360 nm (□), respectively. Decay curves fitted by a bi-exponential law (a) and by a tri-exponential law (b).

Consequently the emission spectrum could be fitting with several bands.

Fig. 9 presents the decay curves measured at room temperature. The excitation wavelengths were selected to favour the relative contribution of these bands in the decay time. Time constants obtained by bi-exponential curve fitting of the emission decays measured at room temperature are $\tau_1 = 0.7\,\mu s$, $\tau_2 = 7.4\,\mu s$ and $\tau_1' = 0.9\,\mu s$, $\tau_2' = 11.4\,\mu s$ for the 310 and 360 nm emissions, respectively (Fig. 9a). It seems that in both emissions, the results obtained by bi-exponential curve fitting do not very well. The use of a tri-exponential curve instead of two improves the results of the fitting (Fig. 9b). The corresponding lifetime values are $\tau_1 = 0.5\,\mu s$, $\tau_2 = 3.8\,\mu s$, $\tau_3 = 12.4\,\mu s$ and $\tau_1' = 0.7\,\mu s$, $\tau_2' = 4.3\,\mu s$, $\tau_3' = 16.6\,\mu s$ for 310 and 360 nm, respectively.

4.2. Discussion

In the structure of $Ag_{0.07}Na_{0.93}Y(PO_3)_4$ crystal, the Ag^+ ion occupies the sodium site. The large coordination number (8) and silver–oxygen bond distances ($2.37 < d(Ag–O) < 2.99$ Å) allow to conclude that the silver–oxygen bond has an ionic character according to the white colour of crystal samples [15] and is consistent with the analysis of the luminescent properties as resulting from ionic silver centres. Most of luminescence works of silver ions have been performed in alkali halide crystals [16], for example, and in crystallized and glassy phosphates [1,17], for example. In these studies, the Ag^+ ion photoluminescence has been related to transitions $4d^{10} \rightarrow 4d^9 5s$. In the present work, the optical spectra show only one inhomogeneous emission in UV. The Stokes shifts of the Ag^+ ion emission correspond to 16,039 cm^{-1} under excitations at 225 nm. This value is larger than that observed in other crystalline phosphates [2], for example 13,000 cm^{-1} for $AgBa(PO_3)_3$ crystal [1]. This is the consequence of the host-lattice stiffness due to the rigid silver–yttrium oxygenated chains or/and it is due to coverings between the emissions and excitations bands, which do not allow determining correctly the maxima of these bands.

The origin of this emission cannot be due to interactions Ag^+–Ag^+ because this optical centre was commonly observed for all structures permitting the formation of $(Ag_2)^{2+}$ pairs [2] induced by a small interatomic Ag^+–Ag^+ distances (~3 Å). In this case, each of them occupies its own site but shares an edge or face with other. In our case, the closest Ag^+–Ag^+ distance is 5.90 Å and the AgO_8 polyhedra are perfectly isolated from the neighbouring silver polyhedra. Each oxygenated silver site shares two faces and one corner with three yttrium polyhedra (Fig. 10). The excitation peak position between 222 and 230 nm agrees with a value of 228.6 nm that is assigned to the parity-forbidden transition d^{10} $(^1S_0) \rightarrow d^9 s(^3D_1)$ in free Ag^+ ion. Moreover, the position of the emission peak between 345 and 360 nm was also similar to those observed previously [1,2] and can be associated to single Ag^+ ion site. On the other hand, the dissymmetry of this emission is a priori not easily interpreted since the structure presents only one silver site and the occupancy possibility of yttrium site by Ag^+ ions must be ruled out. But the weak substitution of Ag^+ ions for Na^+ ions (7%) could produce an inhomogeneous distribution of silver in the sodium site with a slight change of the coordination, such as a decrease of silver site symmetry. This could explain the broad dissymmetric emission band centred to the characteristic emission of isolated Ag^+ ion site.

One can think that these emissions, which translate the various environment of silver, are nearly of the same nature with close temporal characteristics. Indeed, the longer lifetime is of the same order of magnitude as for Ag^+ ions in borate host-lattice (14 μs) in which the silver site symmetry is considered as low [18]. On the

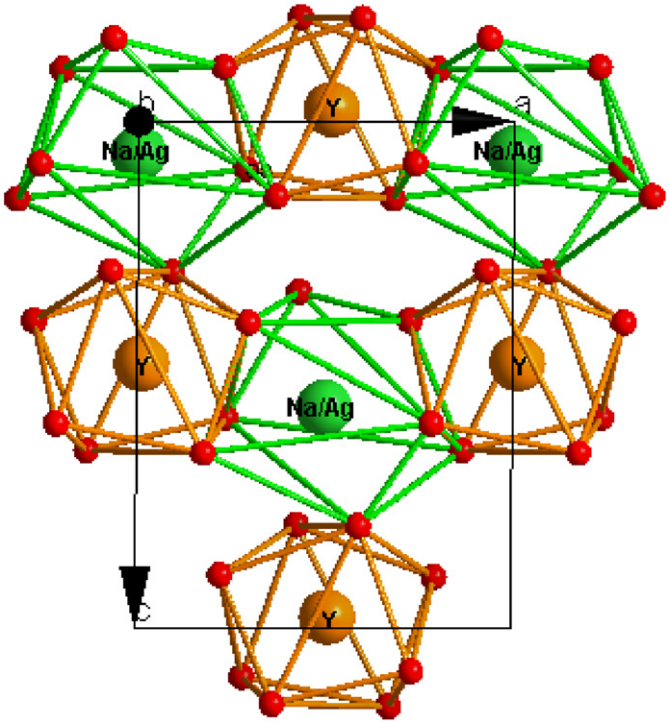

Fig. 10. Representation of the connections of sodium (silver) and yttrium polyhedra in *ab* plane.

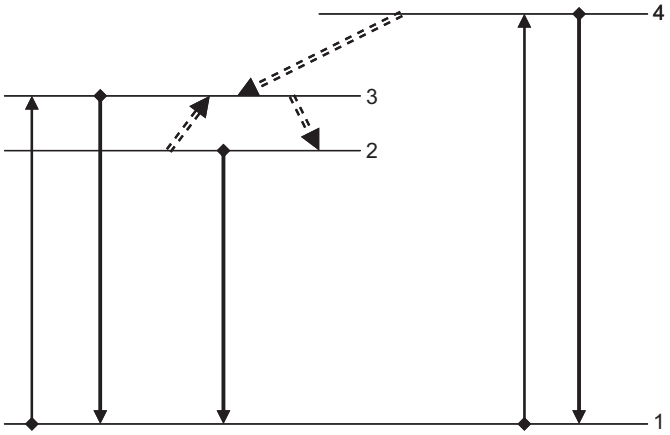

Fig. 11. Four-level system suggested to interpret the decay processes in Ag-doped $NaY(PO_3)_4$ crystal from Borsella et al. [20], see text.

other hand, the fast and the slow lifetime values obtained from this broad band emission can be compared to those reported by Jimenez et al. [19] in the Ag^+-doped aluminophosphate glass. These authors suggested that single Ag^+ ions are the source of this luminescence and interpreted this type of luminescence decay using a four-level system, previously applied to the Ag^+-doped soda–lime glass study [20]. This model (Fig. 11) consists of the ground state (level 1), a singlet state (level 4) directly excited by laser radiation and two close thermalized states (levels 2 and 3). Initially, the level 4 can radiatively decay to the level 1 and can non-radiatively relax to two levels 2 and 3. The fastest ($\tau_1 = 0.5\,\mu s$ and $\tau_1' = 0.7\,\mu s$) lifetime obtained from the tri-exponential fitting should be assigned to the emission from the singlet state (level 4) to the ground state (level 1). After a short time, with respect to the time evolution of the two metastable levels, the upper singlet level is empty, lower levels (2 and 3) are populated and the system behaves as a three-level system. In this context, we suggest that the fast ($\tau_2 = 3.8\,\mu s$ and $\tau_2' = 4.3\,\mu s$) and slow ($\tau_3 = 12.4\,\mu s$ and $\tau_3' = 16.6\,\mu s$) lifetimes of Ag^+ ion emission are likely to be related to the relaxation from metastable upper (level 3) and lower (level 2) states, respectively, to the ground state (level 1).

5. Conclusions

$M^IY(PO_3)_4$ (M^I = Na, Ag) crystallizes in $P2_1/n$ space group (C_{2h}^5 factor group) as the isomorphous $M^ILa(PO_3)_4$ polyphosphates [9]. The JCPDS's PDF card 40-0061 does not correspond to $NaY(PO_3)_4$, the X-ray data given in JCPDS's PDF card 51-0560 shows nearly the same peaks as our results but with a wrong formula of symmetry.

Single crystal $NaY(PO_3)_4$ as silver-doped $Ag_{0.07}Na_{0.93}Y(PO_3)_4$ can be described as built up of no strongly covalent $[YP_4O_{12}]^-$, in between which are located the monovalent cations Na^+ or Ag^+. This structural arrangement induces a great value of the Stokes shifts of luminescence of $Ag_{0.07}Na_{0.93}Y(PO_3)_4$, which supposes a less ionic Ag–O connection compared to other phosphates. Only one dissymmetrical band emits in the UV range with nearly identical temporal characteristics. It is attributed to single Ag^+ ions.

To complete this work, a thermal variation of the lifetime measurements will be performed to elucidate the dynamic of luminescent of the two observed emissions.

Acknowledgments

This work was supported by the "Programme International de Coopération Scientifique du CNRS" (Contract no. 830).

References

[1] I. Belharouak, H. Aouad, M. Mesnaoui, M. Maazaz, C. Parent, B. Tanguy, P. Gravereau, G. Le Flem, J. Solid State Chem. 145 (1999) 97–103.
[2] I. Belharouak, C. Parent, P. Gravereau, J.P. Chaminade, G. Le Flem, B. Moine, J. Solid State Chem. 149 (2000) 284–291.
[3] H. Ettis, H. Naili, T. Mhiri, Cryst. Growth Des. 3 (4) (2003) 599–602.
[4] K. Horchani, J.C. Gâcon, M. Ferid, M. Trabelsi-Ayedi, O. Krachani, G.K. Liu, Opt. Mater. 24 (2003) 169–174.
[5] E.N. Fedorova, L.K. Szmatok, I.I. Kozhina, T.R. Barbanova, Inorg. Mater. Engl. Trans. 22 (1986) 414–418.
[6] W. Szuszkiewiez, Mater. Chem. Phys. 38 (1994) 87–90.
[7] Z. Otwinowski, W. Minor, in: C.W. Carter, R.M. Sweet (Eds.), Methods in Enzymology, Macromolecular Crystallography, vol. 276, Academic Press, London, 1997, pp. 307–326.
[8] G.M. Sheldrick, SHELXL97, A Program for Crystal Structure Refinement, University of Göttingen, Germany, 1997.
[9] M. El Masloumi, I. Imaz, J.P. Chaminade, J.J. Videau, M. Couzi, M. Mesnaoui, M. Maazaz, J. Solid State Chem. 178 (2005) 3581–3588.
[10] H. Koizumi, Acta Crystallogr. B 32 (1976) 2254–2256.
[11] J. Amami, M. Ferid, M. Trabelsi-Ayedi, Mater. Res. Bull. 40 (2005) 2144–2152.
[12] S.I. Maksimova, V.A. Masloboev, K.K. Palkina, A.A. Sazhenkov, N.T. Chibiskova, Russ. J. Inorg. Chem. 33 (1988) 1434–1435.
[13] A. Bertoluzza, in: C. Sandorfy, T. Theophanides (Eds.), Spectroscopy of Biological Molecules, D. Reidel Publishing Company, Dordrecht, 1984, pp. 191–211.
[14] Meyer, H. Hobert, A. Barz, D. Stachel, Vib. Spectrosc. 6 (1994) 323–332.
[15] H.Y.B. Hong, J.A. Kafalas, J.B. Goodenough, J. Solid State Chem. 9 (1974) 345–351.
[16] K. Fussgaenger, Phys. Status Solidi 34 (1969) 157–169;
K. Fussgaenger, Phys. Status Solidi 36 (1969) 645–655.
[17] M. Mesnaoui, C. Parent, B. Tanguy, M. Maazaz, G. Le Flem, Eur. J. Solid State Chem. 29 (1992) 1001–1003.
[18] A. Meijerink, M.M.E. van Heek, G. Blasse, J. Phys. Chem. Solids 54 (8) (1993) 901–906.
[19] J.A. Jimenez, S. Lysenko, G. Zhang, H. Liu, J. Mater. Sci. 42 (2007) 1856–1863.
[20] E. Borsella, G. Battaglin, M.A. Garcia, F. Gonella, P. Mazzoldi, R. Polloni, A. Quaranta, Appl. Phys. A 71 (2000) 125–132.